





Enhancing the population of the encounter complex affects protein complex formation efficiency

Antonella Di Savino¹ , Johannes M. Foerster² , G. Matthias Ullmann²  and Marcellus Ubbink¹ 

¹ Institute of Chemistry, Leiden University, The Netherlands

² Computational Biochemistry, University of Bayreuth, Germany

Keywords

electrostatic interactions; encounter complex; protein–protein interactions

Correspondence

M. Ubbink, Institute of Chemistry, Leiden University, Einsteinweg 55, 2333 CC Leiden, The Netherlands
Tel: +31 71 527 4628
E-mail: m.ubbink@chem.leidenuniv.nl

(Received 9 March 2021, revised 8 July 2021, accepted 16 August 2021)

doi:10.1111/febs.16159

Optimal charge distribution is considered to be important for efficient formation of protein complexes. Electrostatic interactions guide encounter complex formation that precedes the formation of an active protein complex. However, disturbing the optimized distribution by introduction of extra charged patches on cytochrome *c* peroxidase does not lead to a reduction in productive encounters with its partner cytochrome *c*. To test whether a complex with a high population of encounter complex is more easily affected by suboptimal charge distribution, the interactions of cytochrome *c* mutant R13A with wild-type cytochrome *c* peroxidase and a variant with an additional negative patch were studied. The complex of the peroxidase and cytochrome *c* R13A was reported to have an encounter state population of 80%, compared to 30% for the wild-type cytochrome *c*. NMR analysis confirms the dynamic nature of the interaction and demonstrates that the mutant cytochrome *c* samples the introduced negative patch. Kinetic experiments show that productive complex formation is fivefold to sevenfold slower at moderate and high ionic strength values for cytochrome *c* R13A but the association rate is not affected by the additional negative patch on cytochrome *c* peroxidase, showing that the total charge on the protein surface can compensate for less optimal charge distribution. At low ionic strength (44 mM), the association with the mutant cytochrome *c* reaches the same high rates as found for wild-type cytochrome *c*, approaching the diffusion limit.

Introduction

Electrostatic interactions play a major role in protein complex formation. The collision of free proteins in solution can result in early dissociation or lead to the formation of the stereospecific and active complex. Electrostatic interactions can promote the interactions between proteins, guiding the formation of an encounter complex [1–5]. The encounter complex is a very dynamic ensemble of configurations in which proteins sample each other's surface [6]. It can lead to the

formation of the stereospecific and active complex, in which case the encounter is productive [7]. In case of an early dissociation, the encounter is futile [8]. The charge distribution on the surface is considered to be critical to enhance the number of productive encounters, by guiding the incoming partner to the binding site and reducing the surface area to be searched [9]. Previous studies showed how charge mutations can affect the interactions between proteins. For example,

Abbreviations

Cc, cytochrome *c*; CcP, cytochrome *c* peroxidase; CSP, chemical shift perturbations; ET, electron transfer; *I*, ionic strength; k_a , association rate constant; K_D , dissociation constant; MTS, 1-acetoxy-2,2,5,5-tetramethyl-d3-pyrrolidine-3-methyl-methanethiosulfonate; MTSL, 1-oxyl-2,2,5,5-tetramethyl-2,5-dihydropyrrol-3-ylmethyl methanethiosulfonate; PRE, paramagnetic relaxation enhancement.

on the complex formed by TEM1- β -lactamase (TEM1) and its inhibitor, β -lactamase-inhibitor protein (BLIP), charge mutations can enhance the formation of the productive encounter complex resulting in a higher association rate (k_a) but without lowering the dissociation rate. Alternatively, they can alter the encounter complex without any effect on the k_a , or improve the k_a without affecting the encounter complex [7]. Charge mutations can modify the balance of productive and futile encounter complexes, even if located far from the stereospecific binding site. The outcome of the mutation depends on the optimization or interruption of favorable electrostatic ‘pathways’ [10]. The effect of the charged pathways was observed for the complex of cytochrome P450cam and putidaredoxin [11].

Because of their biological functions, electron transfer (ET) proteins often form transient complexes and the charge distribution on their surface is highly optimized to have favorable electrostatic interactions, leading to efficient protein complex formation. These complexes usually have low affinity (dissociation constants, K_D , in the μM – mM range), a consequence of the association and dissociation rate constants both being high. Protein complexes with highly optimized electrostatic interactions have k_a values that approach the limit set by translational diffusion [1]. The ET complex formed by cytochrome *c* (Cc) and cytochrome *c* peroxidase (CcP) from baker’s yeast (*Saccharomyces cerevisiae*) is one of the most studied and best characterized ET complexes. The formation of the complex is guided by electrostatic interactions between the positively charged binding site on Cc and the negatively charges on CcP [12–16]. The encounter state represents 30% of the complex, while 70% is in the stereospecific complex and Cc samples merely 15% of the surface of CcP [17,18]. Several studies have shown that mutations in the interface between Cc and CcP strongly affect association [19–21], so we wondered how important the optimized charge distribution is for the efficiency of the ET reaction. To test this, negative patches were added distant from the stereospecific binding site on CcP, enlarging the surface sampled by Cc in the encounter state. Interestingly, the new negative charges create productive encounters, slightly enhancing the k_a , even if located far from the stereospecific binding site [22,23]. This suggests that the overall charge on CcP surface is more important than the charge distribution. We considered that this could be a consequence of the stability of the stereospecific state as compared to the encounter state. To test this idea, for the current work, we turned to a mutant of Cc, R13A, reported to form a complex with Cc with 80% population of the encounter state [24]. Arg13 has been shown to be a hot spot in the interactions of the

stereospecific complex and its mutation to Ala shifts the balance toward the encounter state and reduces the affinity by 30-fold [24,25]. This mutant was used to study the interaction with native CcP (CcP_A) and a variant of CcP with four Lys residues mutated to Glu on the side of CcP relative to the stereospecific binding site, resulting in a charge change of -8 (CcP_B, Fig. 1) [22,23]. Chemical shift perturbation (CSP) analysis and paramagnetic relaxation enhancement (PRE) experiments show that the complex is highly dynamic and that Cc visits the new negative patch in CcP_B. Kinetic experiments yield reduced association rates for the mutant Cc at moderate and high ionic strength values, but surprisingly, the addition of the negative patch does not reduce the number of productive encounters. At low ionic strength, the mutant Cc associates as fast as wild-type (wt) Cc with CcP. The results are discussed in the context of the importance of charge optimization for complex formation.

Results

The encounter complex formed by CcP on CcR13A is shifted toward Lys4

To compare the CcP encounter complexes of Cc R13A with those of wt Cc, Monte Carlo simulations considering only electrostatic interactions and hard sphere repulsion were performed. Cc wt and R13A interact with the same surface area of CcP, as can be seen in Fig. 2A, in which the centers of mass of Cc are shown around CcP. For CcP_A, the interaction is predominantly around the stereospecific binding site, whereas in CcP_B, the new negative patch is an important site for electrostatic interactions. When reversing the image, showing the centers of mass of CcP around Cc (Fig. 2B), a difference can be observed between Cc wt and R13A. For the former, the main site of interaction is at the C-terminal side of the first α -helix, particularly involving the region close to residues K11 and R13. The mutation of R13 to alanine neutralizes an important positively charged amino acid, causing a shift in the encounter complex. Thus, Cc R13A uses a more extensive surface area to interact with CcP. The same surface is used for the interaction with CcP_A and CcP_B, as can be seen from the similar distributions of the centers of mass for both CcP variants.

The Cc R13A–CcP interaction is predominantly in the encounter state

Binding to CcP causes considerable changes in the amide chemical shifts of Cc [27]. These changes are

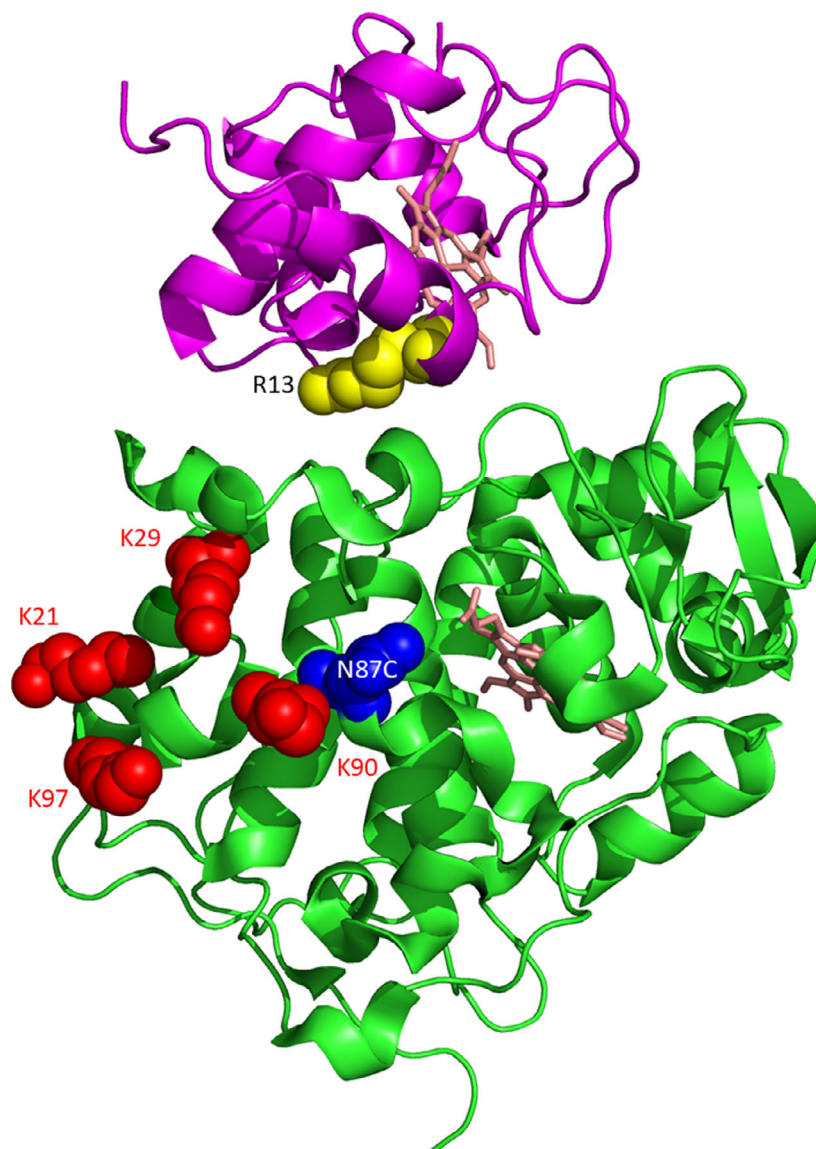


Fig. 1. Mutations in the Cc:CcP complex. The crystal structure of the stereospecific complex formed by Cc (magenta ribbons) and CcP (green ribbons) is shown (PDB 2PCC [12]). The heme groups are shown in salmon sticks, residue R13 is indicated in yellow spacefill representation, the Lys residues that were mutated to Glu to introduce additional negative charges in CcP_B are indicated in red, and residue N87 of CcP mutated to cysteine for spin labeling in blue spacefill. The figure was made with PYMOL [26]. Modified with permission from [22]. Copyright 2021 John Wiley and Sons.

thought to be caused predominantly by the stereospecific complex, as will be discussed later. Cc R13A was shown to shift the equilibrium between encounter and stereospecific states toward the former [24]. In line with those findings, the CSPs observed for the ^{15}N -labeled Cc R13A binding to CcP_A are much smaller than those for wt Cc (Fig. 3A, red bars; Table S1). Also upon binding to CcP_B, the CSPs remain overall smaller for Cc R13A than for wt Cc, indicating that the complex is mainly in the encounter state. Cc R13A interacts with approximately the same surface to CcP_A and CcP_B (Fig. 3B) but differences in the sizes of the CPSs can be observed. The CSP pattern shows several larger perturbations when binding to CcP_B (in the region of residues 5–10 and around

residue 90), suggesting the formation of several more specific interactions. In line with the Monte Carlo simulations, the interface of Cc R13A with CcPA is extended toward Lys4, compared to wt Cc. However, for the complex with CcP_B, this extension is not observed (Fig. 3B).

Cc R13A binds the new patch on CcP_B

To establish whether the introduction of the added negative charges in CcP_B influences the encounter complex with Cc R13A, PRE experiments were performed. CcP_A and CcP_B were tagged with the spin label MTSL after mutating residue N87, which is located close to the added negative patch (Fig. 1), to

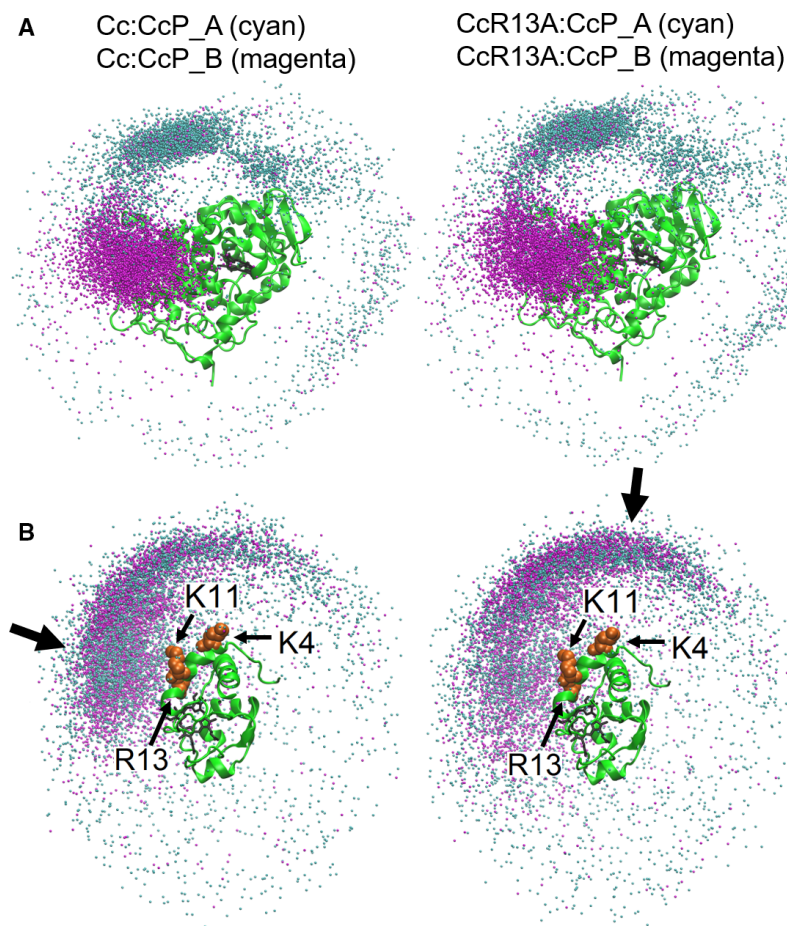


Fig. 2. Monte Carlo simulations of the encounter complex for the Cc:CcP_A, Cc:CcP_B, CcR13A:CcP_A, and CcR13A:CcP_B complexes. The centers of mass of the partner proteins are shown around CcP (A) and Cc (B). The complexes of CcP_A and CcP_B are shown in cyan and magenta, respectively. The heme groups are shown in black sticks. Several charged residues on Cc are colored orange and shown in spacefill. The thick black arrows indicate a difference in the density around wt Cc and Cc R13A. The images were created using VMD [49].

cysteine. The tag causes enhanced relaxation for ^1H nuclear spins in ^{15}N -labeled Cc R13A that come within ~ 2.5 nm of the tag during the interactions with CcP. EPR experiments show that only 15% of the MTSL remained paramagnetic during the tagging reaction (and remains stable afterward). We have observed before that MTSL gets partly reduced during the reaction with CcP, so routinely the paramagnetic fraction was established by EPR [22]. The interaction of Cc with CcP is very fast on the NMR timescale, so all Cc molecules sample many CcP molecules rapidly, averaging the effect of interactions with diamagnetic and paramagnetic CcP molecules. Example spectra are shown in Figs S1 and S2, and Fig. 4 presents the observed PREs for the amides of Cc R13A upon interacting with CcP_A and CcP_B labeled at Cys87 with MTSL. The PREs have been corrected for the 15% paramagnetic labeling by dividing the observed PREs by 0.15. In CcP_A, almost no significant PREs are observed, indicating that Cc R13A does not interact with the surface close to N87. Upon complex formation with CcP_B, large PREs are observed, indicating that Cc R13A visits the region with the extra charges

in proximity of the paramagnetic tag on CcP_B. Clearly, the encounter complex includes the new patch on CcP_B, in line with the findings for wt Cc [22].

Cc R13A reacts more slowly with CcP

To determine whether the R13A mutation in Cc influences the association rate constant with CcP, it was measured as a function of the ionic strength using stopped-flow measurements. Following the work of Miller *et al.* [28], the association rate constant can be measured by observing ET from Cc(Fe^{2+}) to CcP compound I (CpdI), which is formed after reaction with hydrogen peroxide, and example data are given in Fig. S3. The ET rate constant is high, so the observed second-order rate constant is a lower-limit estimate of the association rate constant, as explained in detail in a previous paper [23]; see also Eqn (1) in the **Materials and methods**. The association rate constant for wt Cc to CcP_A and CcP_B is strongly dependent on the ionic strength (Fig. 5, data reproduced from Refs [22,23]), due to the favorable electrostatic interactions between Cc and CcP [29-33]. Following the same

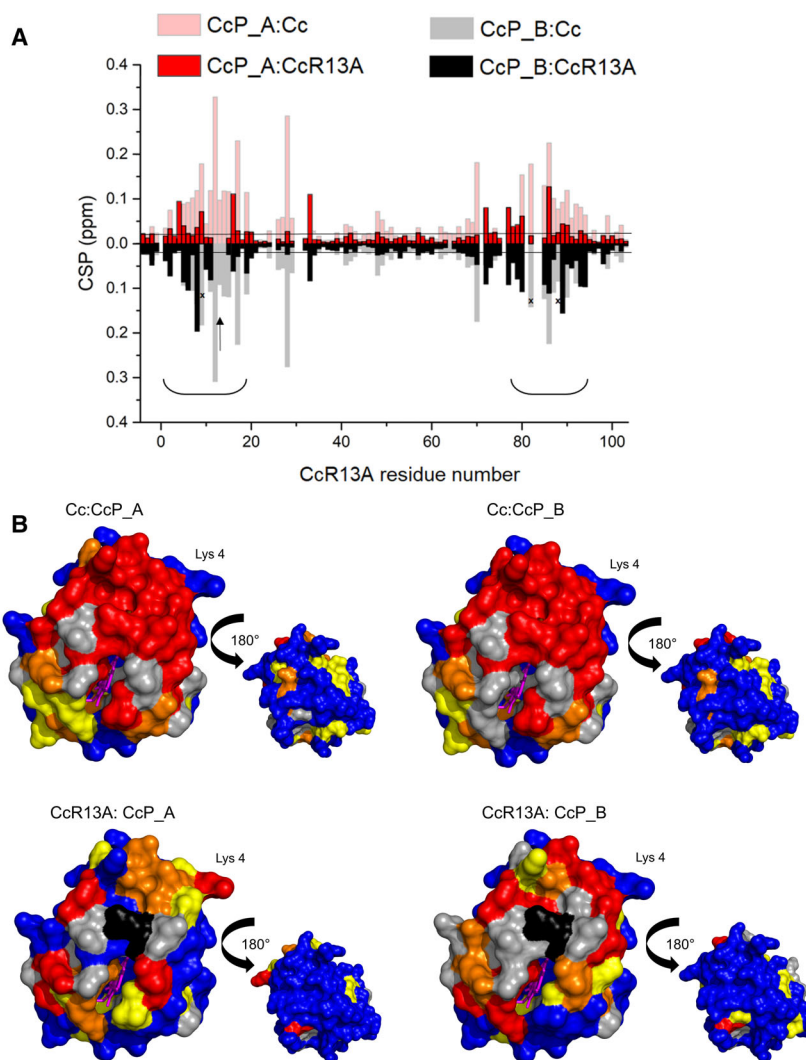


Fig. 3. Chemical shift perturbation upon complex formation. (A) Comparison between the average CSP (see [Materials and methods](#)) for the complexes CcP_A:Cc R13A (in red), CcP_B:Cc R13A (in black), CcP_A:wt Cc (in red shading), and CcP_B:wt Cc (in gray) [22]. The black crosses indicate residues for which data are not available for the complex formed between Cc R13A and CcP_B while they are available for the complex with CcP_A. The horizontal lines indicate the significance threshold at 0.025 p.p.m., and the round brackets indicate the residues involved in the stereospecific binding site; the vertical arrow indicates residue 13. (B) CSP maps for ^{15}N -labeled Cc and CcR13A in complex with CcP_A (left) and CcP_B (right). The surface model of Cc (PDB 2PCC [12]), heme in magenta sticks) is colored according to $\Delta\delta_{\text{avg}} \geq 0.08$ p.p.m. in red, 0.04–0.08 p.p.m. in orange, 0.025–0.04 p.p.m. in yellow, < 0.025 p.p.m. in blue, the residues with no data are in light gray and residue R13 is black in the mutant R13A (See Table S1 for the list of red, orange and yellow residues). The protein structure images were created with PYMOL [26].

approach, the k_a was measured for Cc R13A and CcP_A or CcP_B. In a wide range of ionic strength values, from 122 mM ($11 \text{ mM}^{1/2}$ on the axis of Fig. 5) to 730 mM ($27 \text{ mM}^{1/2}$), the k_a of the complexes formed by Cc R13A is fivefold to sevenfold lower than for the complexes formed by wt Cc (Tables S2–S4). However, curiously, at the lowest ionic strength tested, 44 mM ($7 \text{ mM}^{1/2}$) the k_a of the Cc R13A complexes reaches the same level as those for the complexes formed by wt Cc. We wondered whether the high k_a values at low ionic strength were limited by a technical restraint on measuring very fast rates with stopped-flow. Therefore, the reaction was repeated with half the protein concentrations (Fig. 6). This experiment yielded a slower reaction due to the lower protein concentration. The obtained k_a value was the same as with the higher protein concentrations, showing that the measured rates are not limited by the method and that the

reaction is bimolecular also at low ionic strength. Before, the surprising observation was made that the introduction of a strong negative patch on CcP distant from the stereospecific binding site did not lower the k_a for wt Cc, but rather increased it somewhat [23]. Similarly, for Cc R13A, we observe that the formation of the ET active complex is not slowed down by the additional charges on CcP_B, as compared to CcP_A (Fig. 5).

Discussion

Volkov *et al.* [24] showed that the Cc mutation Arg13 to Ala drastically increases the population of the encounter complex with CcP, from 30% to 80%. Also, the binding constant (K_B) decreases from $1.9 \times 10^5 \text{ M}^{-1}$ of the wt complex to $0.06 \times 10^5 \text{ M}^{-1}$ for Cc R13A bound to CcP. We previously reported that the

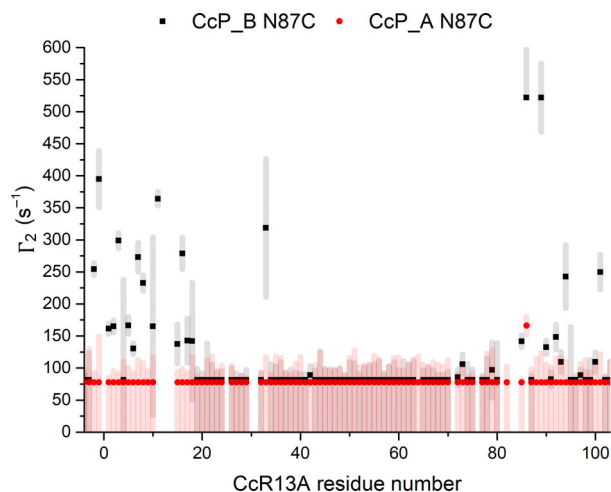


Fig. 4. Probing new interactions with PRE NMR. The PREs are shown for amide nuclear spins of Cc R13A in the presence of CcP_A (in red) or CcP_B (in black), tagged with MTSL at Cys87, which is located close to the negative patch added on CcP_B. The error bars are indicated as shaded regions and represent the propagated 2x SD errors of the raw data. The observed PREs were divided by 0.15 to correct for the fraction of CcP that was paramagnetic (see text).

addition of a negative patch on a side of the binding site of CcP (CcP_B) enlarges the area sampled by Cc in the encounter complex. Since the k_a for Cc and CcP_B is slightly higher than that for the wt complex, it was concluded that the added charges result in more productive encounters [22]. The aim of the present study was to investigate to what degree the delicate balance between stereospecific complex and encounter complex influences the association between Cc and CcP by comparing the interactions between CcP with wt Cc and Cc R13A.

The CSP analysis shows that Cc R13A forms a more dynamic complex with both CcP_A and CcP_B than does wt Cc, in line with a more populated encounter state, because the CSPs overall are smaller. Previous studies have indicated that the magnitude of the CSPs after correction for the fraction bound correlates with the dynamics in transient protein complexes. Small shift perturbations indicate a strongly populated encounter complex, at least in dynamic, short-lived complexes of ET proteins. The rationale is that in the encounter complex, many orientations are averaged, reducing the average CSP, and that in the encounter state, the proteins are still solvated and thus resemble the free state, whereas in a stereospecific complex, partial desolvation and specific interactions cause larger CSP [24,34,35,36]. The Cc R13A CSP patterns obtained with the two variants of CcP are not the same, contrary to the finding for wt Cc (Fig. 3B) [22].

In the latter, the stereospecific complex is more populated and the main contributor to the CSP. The CSP differences observed for Cc R13A indicate differences in the interactions with CcP_A and CcP_B. This observation is further supported by the PRE results that show clearly that the region with the new negative patch in CcP_B is visited by Cc R13A. It does not do so in the complex with CcP_A, in accord with the Monte Carlo simulations, this work and Ref. [24], which show that the encounter complexes of wt Cc and Cc R13A with CcP_A involve the surface area of CcP around the stereospecific binding site.

To test to what degree the increased dynamics in the complexes formed by Cc R13A influence the formation of the active complex, the k_a for binding to CcP_A or CcP_B was determined. The favorable electrostatic interactions between Cc R13A and the CcP variants cause a strong ionic strength dependence of k_a . At an ionic strength of 122 mM and higher, the k_a values for the complexes formed by Cc R13A are fivefold to sevenfold lower than for wt Cc at the same ionic strength. Surprisingly, at the lowest ionic strength tested, 44 mM, the k_a of the complexes formed by Cc R13A and either CcP variants reaches the k_a of the complexes formed by wt Cc. So, whereas the rate constant plateaus at low ionic strength for wt Cc, the one for Cc R13A monotonically increases.

The plateau reached for wt Cc can have various reasons. It could be that monopole–dipole interactions may come into play [37,38] at low ionic strength that work against each other and cause the leveling off of

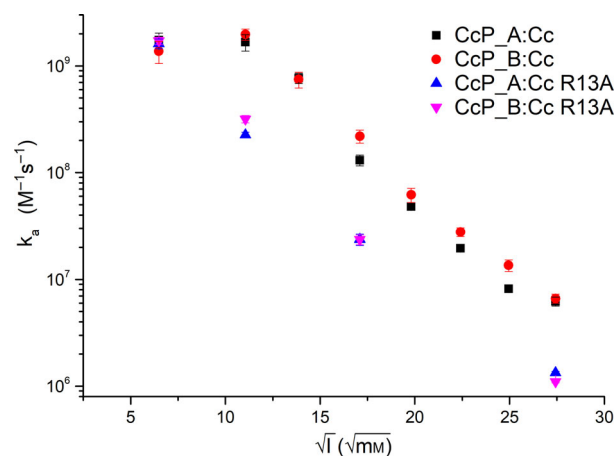
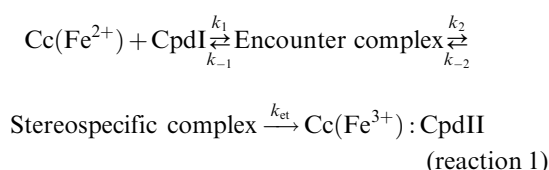


Fig. 5. Rate of association (k_a) between the Cc and CcP variants. The k_a values, plotted as a function of the square root of the ionic strength, were obtained from the simulations of the stopped-flow kinetics. Errors were calculated as the standard deviation between at least three replicates and simulations performed at different CcP concentrations (see [Materials and methods](#) for details).

the k_a . However, this effect is observed for CcP_A and CcP_B and even for CcP_D, which has a strong new negative patch at the far end from the stereospecific binding site [23]. These three variants have widely different dipoles, yet all show the same behavior. Alternatively, at $I = 122$ mM the diffusion limit may be reached with k_a is $2 \times 10^9 \text{ M}^{-1} \cdot \text{s}^{-1}$ for wt Cc binding to CcP_A, so increasing the charge interactions further does not result in faster association. A third explanation is that the encounter complex, which is dominated by electrostatic interactions, is the most favorable state at low ionic strength, and thus, the balance between encounter and stereospecific complex shifts to the former at low ionic strength, reducing the fraction of the active complex. Such ‘inhibition’ by strong charge interactions outside the stereospecific binding site has been proposed before [39–42]. It is not trivial to determine which of the two explanations is applicable here. We used simulation of complex formation to evaluate ranges that the k_a values can assume. Details are given in the Text S1.



The association reaction can be described by reaction 1, in which CpdII refers to compound II, the second intermediate in the reduction in hydrogen peroxide by CcP. Cc and CcP associate to form the encounter complex, which can evolve to the stereospecific complex, in which ET can occur. The simulation shows for wt Cc that an increase in k_1 above the k_a measured at $I = 122$ mM must be accompanied by a substantially increased population (from 30% to > 90%) of the encounter state to obtain the experimental k_a value at $I = 44$ mM, which is nearly the same as the one at $I = 122$ mM (Table S5). So, either the diffusion limit is reached or the complex indeed becomes ‘locked’ at low ionic strength in the electrostatically stabilized encounter state, reducing the fraction of ET active complex.

The kinetic results for Cc R13A were also simulated. At $I = 122$ mM, the K_B value, the population of the encounter complex and the k_a values have been reported for both wt Cc and Cc R13A in complex with CcP_A ([23,24], this work), restraining the microscopic rate constants in reaction 1 (Table S5). Simulation shows that the sevenfold lower k_a value observed for Cc R13A is attributable to a combination of a lower k_1 and the lower population of the stereospecific complex (implying that the second equilibrium is more to

the left). Cc R13A lacks the positive side chain of Arg13 in the binding interface, so a lowered k_1 is to be expected, because of weaker electrostatic interactions. The k_a observed for Cc R13A at 44 mM can be found by increasing k_1 and lowering k_{-1} without changing the population of the encounter state. Thus, it seems that at $I = 44$ mM the wt Cc complex could become structurally and kinetically similar to the complex formed with Cc R13A, with a more populated encounter state.

Conclusions

The CSP data confirm that the mutation of the Arg 13 of Cc to Ala enhances the dynamic component in the binding with the CcP variants. While it was shown that the binding mode of wt Cc with CcP_A and CcP_B is the same [22], the interactions of Cc R13A with CcP_B vary more from those with CcP_A and are somewhat more specific. Paramagnetic relaxation enhancement experiments showed that, similarly to what shown for the Cc:CcP_B complex [22], the added charges enlarge the surface of CcP visited by Cc R13A. The new patch disturbs the optimized charge distribution on the surface of CcP, yet it does not result in less productive encounters because the association rate constant is not reduced. Stopped-flow experiments were used to evaluate the influence of the higher population of encounter state on the association rate between Cc R13A and the CcP variants. At ionic strength values above 122 mM ($11 \text{ mM}^{1/2}$), the k_a exhibits a fivefold to sevenfold reduction compared to wt Cc, indicating that the population of the encounter state has a role in balancing dynamics and specificity in the protein complex formation, and thus can be critical for the efficiency of ET.

Materials and methods

Monte Carlo simulations

The structures of CcP and Cc were taken from the PDB 2PCC [12], and hydrogen atoms were added with the module HBUILD [43] of the program CHARMM [44]. The positions of the hydrogen atoms were minimized using CHARMM force field [45] while all heavy atoms were kept fixed. Four point mutations were introduced for the mutant CcP B, as was done in the experiment: K21E, K29E, K90E, and K97E using the program PYMOL [26]. For the mutant CcR13A, a point mutation was introduced as was done for CcP_B. The heme molecules of CcP and Cc were considered to be in the oxidized state. The electrostatic potential of CcP was calculated using the program APBS [46] with a dielectric

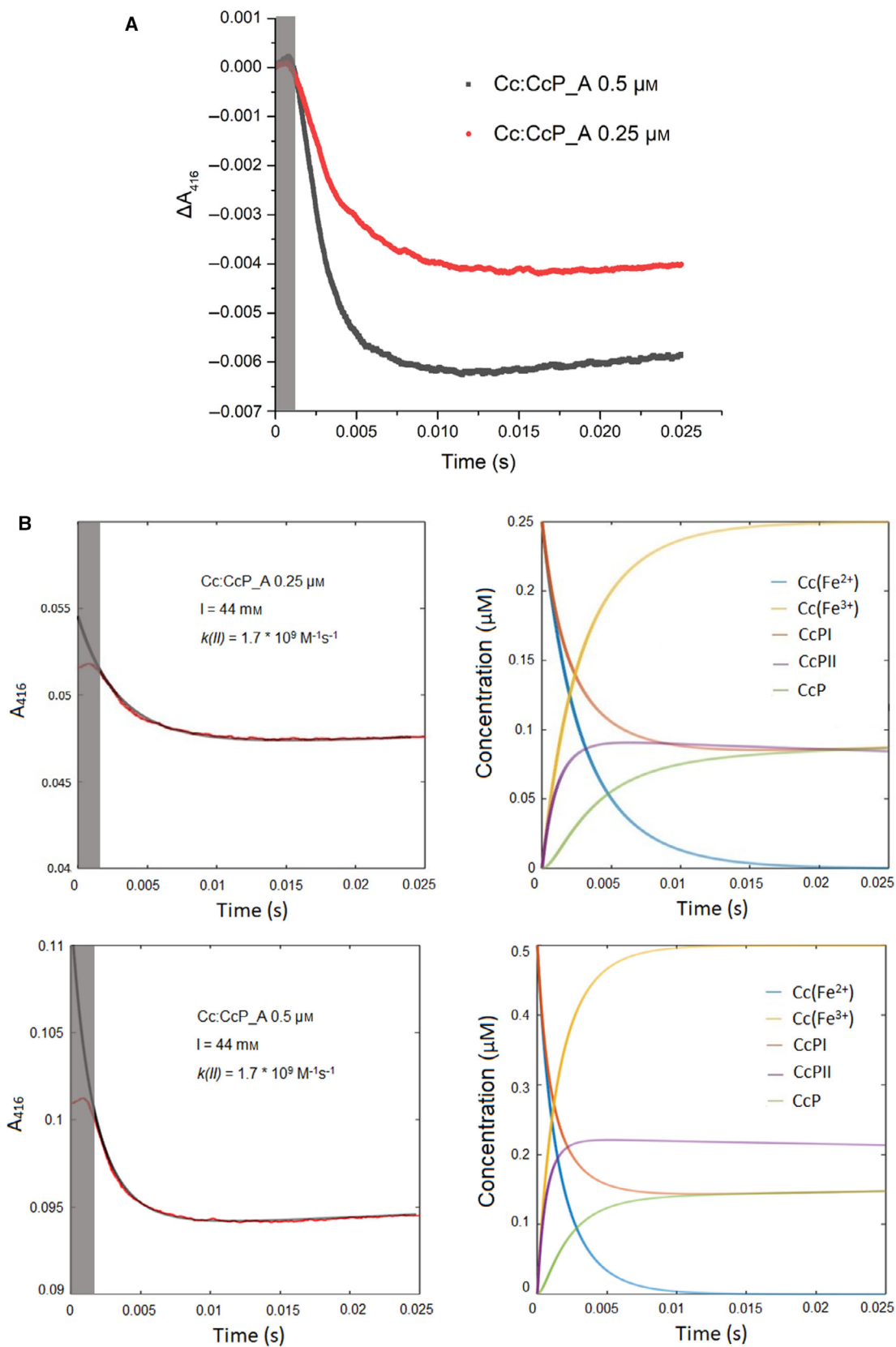


Fig. 6. Electron transfer between Cc(II) and CpdI of CcP_A at an ionic strength of 44 mM at two protein concentrations. The area in gray relates to an artifact caused by the stopped-flow excluded from the analysis. (A) The reaction curve between Cc and CcP_A with both the proteins at 0.5 μM is shown in black, the one with both proteins 0.25 μM in red. (B) Simulations of the kinetics measured for Cc and CcP_A at 0.5 and 0.25 μM . On the left, the experimental data are shown in red and the simulation in black. On the right, the change in concentration of all species involved in the Cc:CcP cycle based on the simulation is shown as a function of time.

constant of 4.0 for the protein and 80 for water, respectively, in which 120 mM NaCl was dissolved. The temperature was set to 303 K. The electrostatic potentials were saved on a grid with the dimension $(22.5 \text{ nm})^3$.

The electrostatic docking procedure was done using the program suite MCMAP [47]. The protein CcP was considered as receptor and the ligand Cc or CcR13A moved randomly in the electrostatic field of CcP. The Metropolis Monte Carlo simulation [48] consisted of 250 runs with 10^6 steps each at a temperature of 303 K. Different ensembles of the encounter complex were created in which encounters within a distance of 0.3 nm to the surface of CcP or without a distance criterion were considered as valid encounter. For each resulting ensemble, 5000 randomly chosen encounters were used for further analysis. Each individual ensemble was visually analyzed for distribution and the formation of encounter clusters with VMD [49].

Sample preparation

Saccharomyces cerevisiae Cc and CcP (both EC 1) and their variants Cc R13A and CcP_B were expressed and purified as previously described [17,22,25,50,51]. The EPR and the PRE experiments were performed as previously reported [18,22,51]. Briefly, CcP was tagged with either MTS [(1-acetoxy-2,2,5,5-tetramethyl-d3-pyrroline-3-methyl)-methanethiosulfonate] as diamagnetic tag (TRC, Canada) or MTSL [(1-oxyl-2,2,5,5-tetramethyl-d3-pyrroline-3-methyl)-methanethiosulfonate] (ChemCruz, Santa Cruz Biotechnology, Dallas, TX, USA) as paramagnetic tag. To perform the labeling, single cysteine CcP mutants were reduced incubating the sample with 10 mM DTT in argon bubbled 20 mM sodium phosphate, 0.1 M NaCl pH 6, at 4 °C for 1 h. A PD10 column was used to eliminate the excess of DTT. The protein was eluted directly in a solution of MTSL (or MTS) in 20 : 1 ratio tag on protein concentration in 20 mM sodium phosphate, 0.1 M NaCl, pH 6.0 and incubated under argon flow at 4 °C for 30 min. The excess of free tag was eliminated through gel filtration. For PRE experiments, two ^{15}N - ^1H BEST-TROSY-HSQC [52] of the oxidized ^{15}N CcR13A were recorded, one with the paramagnetic MTSL-tagged CcP and one with the diamagnetic MTS-tagged CcP. CcR13A and CcP were mixed in a 1 : 1 ratio at 200 μM in 20 mM sodium phosphate, 0.1 M NaCl, pH 6.0. The spectra were recorded on a AVIII HD 850 MHz spectrometer (Bruker, Karlsruhe, Germany) at 293 K with 0.333-s relaxation delay, 64 scans and 1048 and 200 complex points in the ^1H

and ^{15}N dimensions, respectively. The PREs were calculated according to the formula:

$$\frac{I_{\text{para}}}{I_{\text{dia}}} = \frac{R_2 e^{-tR_2}}{R_2 + \Gamma_2},$$

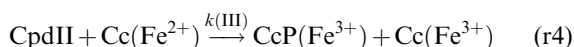
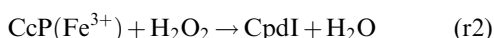
where I_{para} and I_{dia} are the peak intensities in the HSQC spectra of the paramagnetic and diamagnetic samples, respectively, R_2 is the transverse relaxation rate of Cc R13A, Γ_2 is the PRE, and t is the total INEPT evolution time of the HSQC [53]. For PRE analysis, two sets of transverse relaxation rates of the diamagnetic sample were obtained: One was obtained using CCPN analysis version 2.4.0 and the second one fitting the resonances to a Lorentzian line shape using FuDA (kindly previously provided by D. Fleming Hansen, University College London). The two sets of R_2 values were averaged to obtain the final R_2 , and their standard deviation was reported as error. The PREs were corrected for the percentage of paramagnetic signal of the MTSL-tagged CcP (15% for both CcP_A and CcP_B, see Results) and for the fraction of Cc bound to CcP. The percentage of Cc R13A bound to CcP was calculated using the previously reported binding constant: $0.06 \pm 0.002 \times 10^5 \text{ M}^{-1}$ [25]. The paramagnetic fraction of CcP was measured through EPR before the PRE experiment. For the EPR measurement, two samples were prepared in 20 mM sodium phosphate, 0.1 M NaCl, pH 6.0. One sample contained 140 μM MTSL-tagged CcP and the other one 100 μM freshly dissolved free MTSL used as reference. The double integral of the two EPR spectra was compared normalizing for the difference in MTSL concentration. The error in the EPR measurement is estimated to be ± 5 percent points. The measurements were performed at 9.8 GHz, at room temperature, using 0.63 mW microwave power, 2 G modulation amplitude, 100 kHz modulation frequency, and a time constant of 10.24 ms [22]. The assignment of the ^{15}N Cc R13A HSQC was obtained comparing the spectrum with the assignment of the wt Cc spectrum [54–56] (BMRB 17845). Several residues, mostly around the mutation site, could not be assigned. The CSPs were measured by overlaying the HSQC spectra of Cc R13A bound to CcP tagged with the diamagnetic tag MTS to the spectrum of free Cc R13A. The average CSP were calculated as weighted average between the chemical shifts in the proton and nitrogen dimensions using the formula:

$\{0.5[(\Delta_{\text{NH}})^2/25]+0.5(\Delta_{\text{H}})^2\}^{1/2}$ where Δ_i is the chemical shift difference for the resonance i for the bound and free protein [57].

Kinetic experiments

The kinetic data on the Cc:CcP_A and Cc:CcP_B complexes were published in our previous works [22,23]. The same protocol and analysis were performed to measure the reactions between CcR13A and the two CcP variants at 752, 292, 122, and 44 mM ionic strength. Shortly before each measurement, CcR13A was reduced with sodium ascorbate in 20 mM sodium phosphate solution, 270 mM NaCl, pH 8. PD10 columns were used to eliminate the excess of ascorbate and to exchange the buffer of CcR13A and CcP solutions to 20 mM sodium phosphate solution pH 6 and NaCl up to the desired ionic strength: 752, 292, 122, or 44 mM taking into account the contribution of the phosphate. All the reactions were performed mixing equimolar solutions of CcR13A and CcP to a final concentration of 0.5 μM for both proteins. The reaction at 44 mM ionic strength was also performed with a final concentration of 0.25 μM of both Cc and CcP. All the kinetics were measured at room temperature on a SX20 stopped-flow spectrometer (Applied Photophysics, Leatherhead, Surrey, UK) with a 1.2-ms dead time, following the oxidation of Cc at 416 nm. In order to have a good signal-to-noise ratio, each kinetic curve resulted from the average of 14 single measurements.

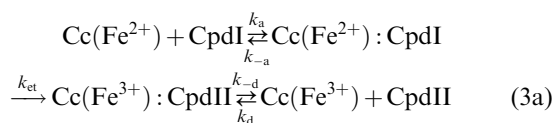
During the catalytic cycle, two molecules of Cc sequentially reduce CcP transferring one electron at the time.



Upon reduction in hydrogen peroxide, CcP is converted to CpdI (r2), which receives one electron from Cc forming CpdII (r3). Finally, CpdII accepts a second electron from a second molecule of Cc restoring the resting state of CcP [58]. All the reactions involving the oxidation of Cc contribute to the change in absorbance at 416 nm (r3 and r4). The conversion of CpdI in CpdII consists in the reduction in the Trp radical, which does not cause any spectral change in the visible light. The measurement of the kinetics at a ratio 1 : 1 between Cc(II) and CpdI allows other reactions between different species formed during the cycle to happen. Specifically, when CpdII is formed in r3, the dismutation reaction between two CpdII molecules can occur:



Right at the beginning of the stopped-flow measurement, the first fast decay of the kinetic curve is caused by reaction 3 which can be expanded as follows:



The change in absorbance at 416 nm indicates the oxidation of Cc, and therefore, it can be observed after the electron transfer step (k_{et}). Thus, the observed rate constant in the kinetic curve, k_{obs} , describes the first two parts of reaction 3a. Under pseudosteady state conditions ($\partial\text{Cc}(\text{Fe}^{2+}) : \text{CpdI} / \partial t = \partial\text{Cc}(\text{Fe}^{3+}) : \text{CpdII} / \partial t = 0$), Eqn (1) correlates the simulated rate $k(\text{II})$ and the association rate constant k_a :

$$k(\text{II}) = \frac{k_a k_{\text{et}}}{k_{-a} + k_{\text{et}}} \quad (1)$$

For wt Cc and CcP, the electron transfer rate (k_{et}) is known to be much larger than the dissociation rate (k_{-a}), so the observed $k(\text{II})$ can be used as a good approximation of the association rate k_a , $k(\text{II}) \approx k_a$ [1,59]. Otherwise, $k(\text{II})$ represents a lower limit for the association rate constant k_a . In order to obtain the $k(\text{II})$, each kinetic curve was simulated using GNU Octave [60]. The script is available in the SI of our previous work [23]. The change in concentration of the different species present in solution during the reaction cycle was simulated using the following differential equations:

$$\begin{aligned} \frac{d[\text{Cc}(\text{Fe}^{2+})]}{dt} &= -k(\text{II}) * [\text{Cc}(\text{Fe}^{2+})] * [\text{CpdI}] - k(\text{III}) * \\ &[\text{Cc}(\text{Fe}^{2+})] * [\text{CpdII}], \end{aligned} \quad (2)$$

$$\frac{d[\text{CpdI}]}{dt} = -k(\text{II}) * [\text{Cc}(\text{Fe}^{2+})] * [\text{CpdI}] + k(\text{IV}) * [\text{CpdII}]^2, \quad (3)$$

$$\begin{aligned} \frac{d[\text{Cc}(\text{Fe}^{3+})]}{dt} &= k(\text{II}) * [\text{Cc}(\text{Fe}^{2+})] * [\text{CpdI}] + k(\text{III}) * \\ &[\text{Cc}(\text{Fe}^{2+})] * [\text{CpdII}], \end{aligned} \quad (4)$$

$$\begin{aligned} \frac{d[\text{CpdII}]}{dt} &= k(\text{II}) * [\text{Cc}(\text{Fe}^{2+})] * [\text{CpdI}] - k(\text{III}) * \\ &[\text{Cc}(\text{Fe}^{2+})] * [\text{CpdII}] - k(\text{IV}) * [\text{CpdII}]^2, \end{aligned} \quad (5)$$

$$\frac{d[\text{CcP}]}{dt} = k(\text{IV}) * [\text{CpdII}]^2 + k(\text{III}) * [\text{Cc}(\text{Fe}^{2+})] * [\text{CpdII}]. \quad (6)$$

The kinetic curve measured at the stopped-flow is recreated summing the contributions of each species to the absorbance at 416 nm according to the Beer-Lambert law:

$$A_{416} = \epsilon_{\text{Cc(Fe}^{2+})} * [\text{Cc(Fe}^{2+})] + \epsilon_{\text{CpdI}} * [\text{CpdI}] + \epsilon_{\text{Cc(Fe}^{3+})} * [\text{Cc(Fe}^{3+})] + \epsilon_{\text{CpdII}} * [\text{CpdII}] + \epsilon_{\text{CcP}} * [\text{CcP}] + C, \quad (7)$$

where C is a parameter manually optimized for the baseline correction. The extinction coefficients at 416 nm are $129.1 \text{ mM}^{-1} \cdot \text{cm}^{-1}$ for Cc(Fe²⁺) [61], $88.8 \text{ mM}^{-1} \cdot \text{cm}^{-1}$ for Cc(Fe³⁺) [61], and for CcP and CpdI as previously reported in [23]. The values of $k(\text{II})$, $k(\text{III})$, and $k(\text{IV})$ were independently changed manually until the simulation was considered a good fit as judged by visual observation. The main source of error for this experiment is the error in concentration of the two proteins mixed in the stopped-flow apparatus. A maximum deviation of 20% from the theoretical concentration was measured. As a consequence, the presented k_a values at each ionic strength are calculated as the average of at least three kinetic curve replicates, simulated at the expected experimental concentration and at a concentration of CcP 20% lower. The error of the rates were calculated as the standard deviation between the association rates at each salt concentration [23]. The *t*-test analysis for significance in difference of k_a values is given in Tables S3 and S4.

Acknowledgements

This work was supported by the Netherlands Organization for Scientific Research (NWO-CW grant 711.013.007 to MU) and by the Deutsche Forschungsgemeinschaft (DFG, German Research Foundation—Project Number 391977956—SFB 1357 to GMU) and the study program ‘Biological Physics’ of the Elite Network of Bavaria (JMF and GMU).

Conflict of interest

The authors declare no conflict of interest.

Author contributions

ADS, JMF, GMU, and MU performed research, analyzed data, and wrote the paper.

Peer review

The peer review history for this article is available at <https://publons.com/publon/10.1111/febs.16159>.

References

- Schreiber G, Haran G & Zhou HX (2009) Fundamental aspects of protein-protein association kinetics. *Chem Rev* **109**, 839–860.
- Ubbink M (2012) Dynamics in transient complexes of redox proteins. *Biochem Soc Trans* **40**, 415–418.
- Yang J, Zeng Y, Liu Y, Gao M, Liu S, Su Z & Huang Y (2020) Electrostatic interactions in molecular recognition of intrinsically disordered proteins. *J Biomol Struct Dyn* **38**, 4883–4894.
- Zhou HX & Pang X (2018) Electrostatic interactions in protein structure, folding, binding, and condensation. *Chem Rev* **118**, 1691–1741.
- Clore GM (2014) Interplay between conformational selection and induced fit in multidomain protein-ligand binding probed by paramagnetic relaxation enhancement. *Biophys Chem* **186**, 3–12.
- Schilder J & Ubbink M (2013) Formation of transient protein complexes. *Curr Opin Struct Biol* **23**, 911–918.
- Harel M, Spaar A & Schreiber G (2009) Fruitful and futile encounters along the association reaction between proteins. *Biophys J* **96**, 4237–4248.
- Fawzi NL, Doucleff M, Suh JY & Clore GM (2010) Mechanistic details of a protein-protein association pathway revealed by paramagnetic relaxation enhancement titration measurements. *Proc Natl Acad Sci USA* **107**, 1379–1384.
- Adam G & Delbrück M (1968) Reduction of dimensionality in biological diffusion processes. In *Structural Chemistry and Molecular Biology* (Rich A & Davidson N, eds), p. 198. W. H. Freeman and Co., San Francisco, CA.
- An SY, Kim E-H & Suh J-Y (2018) Facilitated protein association via engineered target search pathways visualized by paramagnetic NMR spectroscopy. *Structure* **26**, 887–893.e2.
- Andraøjć W, Hiruma Y, Liu WM, Ravera E, Nojiri M, Parigi G, Luchinat C & Ubbink M (2017) Identification of productive and futile encounters in an electron transfer protein complex. *Proc Natl Acad Sci USA* **114**, E1840–E1847.
- Pelletier H & Kraut J (1992) Crystal structure of a complex between electron transfer partners, cytochrome *c* peroxidase and cytochrome *c*. *Science* **258**, 1748–1755.
- Gabdoulline RR & Wade RC (2001) Protein-protein association: investigation of factors influencing association rates by Brownian dynamics simulations. *J Mol Biol* **306**, 1139–1155.
- Poulos TL, Freer ST, Alden RA, Edwards SL, Skogland U, Takio K, Eriksson B, Xuong NH, Yonetani T & Kraut J (1980) Crystal-structure of cytochrome-*c* peroxidase. *J Biol Chem* **255**, 575–580.
- Louie GV, Hutcheon WLB & Brayer GD (1988) Yeast iso-1-cytochrome *c*: A 2.8 Å resolution three-dimensional structure determination. *J Mol Biol* **199**, 295–314.
- Northrup SH, Boles JO & Reynolds JC (1988) Brownian dynamics of cytochrome *c* and cytochrome *c* peroxidase association. *Science* **241**, 67–70.

- 17 Volkov AN, Worrall JAR, Holtzmann E & Ubbink M (2006) Solution structure and dynamics of the complex between cytochrome *c* and cytochrome *c* peroxidase determined by paramagnetic NMR. *Proc Natl Acad Sci USA* **103**, 18945–18950.
- 18 Bashir Q, Volkov AN, Ullmann GM & Ubbink M (2010) Visualization of the encounter ensemble of the transient electron transfer complex of cytochrome *c* and cytochrome *c* peroxidase. *J Am Chem Soc* **132**, 241–247.
- 19 Erman JE, Vitello LB, Pearl NM, Jacobson T, Francis M, Alberts E, Kou A & Bujarska K (2015) Binding of yeast cytochrome *c* to forty-four charge-reversal mutants of yeast cytochrome *c* peroxidase: isothermal titration calorimetry. *Biochemistry* **54**, 4845–4854.
- 20 Pearl NM, Jacobson T, Arisa M, Vitello LB & Erman JE (2007) Effect of single-site charge-reversal mutations on the catalytic properties of yeast cytochrome *c* peroxidase: mutations near the high-affinity cytochrome *c* binding site. *Biochemistry* **46**, 8263–8272.
- 21 Pearl NM, Jacobson T, Meyen C, Clementz AG, Ok EY, Choi E, Wilson K, Vitello LB & Erman JE (2008) Effect of single-site charge-reversal mutations on the catalytic properties of yeast cytochrome *c* peroxidase: evidence for a single, catalytically active, cytochrome *c* binding domain. *Biochemistry* **47**, 2766–2775.
- 22 Di Savino A, Foerster J, La Haye T, Blok A, Timmer M, Ullmann M & Ubbink M (2020) Efficient encounter complex formation and electron transfer to cytochrome *c* peroxidase with an additional, distant electrostatic binding site. *Angew Chem Int Ed Engl* **132**, 23239–23243.
- 23 Di Savino A, Foerster JM, Ullmann GM & Ubbink M (2021) The charge distribution on a protein surface determines whether productive or futile encounter complexes are formed. *Biochemistry* **60**, 747–755.
- 24 Volkov AN, Bashir Q, Worrall JAR, Ullmann GM & Ubbink M (2010) Shifting the equilibrium between the encounter state and the specific form of a protein complex by interfacial point mutations. *J Am Chem Soc* **132**, 11487–11495.
- 25 Volkov AN, Bashir Q, Worrall JAR & Ubbink M (2009) Binding hot spot in the weak protein complex of physiological redox partners yeast cytochrome *c* and cytochrome *c* peroxidase. *J Mol Biol* **385**, 1003–1013.
- 26 Schrödinger L. The PyMOL molecular graphics system, version 1.3.
- 27 Worrall JAR, Kolczak U, Canters GW & Ubbink M (2001) Interaction of yeast iso-1-cytochrome *c* with cytochrome *c* peroxidase investigated by N-15, H-1 heteronuclear NMR spectroscopy. *Biochemistry* **40**, 7069–7076.
- 28 Miller MA, Liu RQ, Hahm S, Geren L, Hibdon S, Kraut J, Durham B & Millett F (1994) Interaction domain for the reaction of cytochrome *c* with the radical and the oxyferryl heme in cytochrome *c* peroxidase compound I. *Biochemistry* **33**, 8686–8693.
- 29 Zhou JS & Hoffman BM (1994) Stern-Volmer in reverse - 2/1 stoichiometry of the cytochrome *c* cytochrome *c* peroxidase electron-transfer complex. *Science* **265**, 1693–1696.
- 30 Van de Water K, Sterckx YGJ & Volkov AN (2015) The low-affinity complex of cytochrome *c* and its peroxidase. *Nat Commun* **6**, 7073.
- 31 Matthis AL & Erman JE (1995) Cytochrome *c* peroxidase-catalyzed oxidation of yeast iso-1 ferrocyclochrome *c* by hydrogen peroxide. Ionic strength dependence of the steady-state parameters. *Biochemistry* **34**, 9985–9990.
- 32 Matthis AL, Vitello LB & Erman JE (1995) Oxidation of yeast iso-1 ferrocyclochrome *c* by yeast cytochrome *c* peroxidase compounds I and II. Dependence upon ionic strength. *Biochemistry* **34**, 9991–9999.
- 33 McLendon G, Zhang Q, Billstone V, Wallin SA, Miller RM, Spears KG & Hoffman BM (1993) Thermodynamic and kinetic aspects of binding and recognition in the cytochrome *c*/cytochrome *c* peroxidase complex. *J Am Chem Soc* **115**, 3665–3669.
- 34 Worrall JAR, Reinle W, Bernhardt R & Ubbink M (2003) Transient protein interactions studied by NMR spectroscopy: the case of cytochrome *c* and adrenodoxin. *Biochemistry* **42**, 7068–7076.
- 35 Volkov AN, Ferrari D, Worrall JAR, Bonvin AMJJ & Ubbink M (2005) The orientations of cytochrome *c* in the highly dynamic complex with cytochrome *b* 5 visualized by NMR and docking using HADDOCK. *Protein Sci* **14**, 799–811.
- 36 Xu XF, Reinle WG, Hannemann F, Konarev PV, Svergun DI, Bernhardt R & Ubbink M (2008) Dynamics in a pure encounter complex of two proteins studied by solution scattering and paramagnetic NMR spectroscopy. *J Am Chem Soc* **130**, 6395–6403.
- 37 Van Leeuwen JW (1983) The ionic strength dependence of the rate of a reaction between two large proteins with a dipole moment. *Biochim Biophys Acta* **743**, 408–421.
- 38 Watkins JA, Cusanovich MA, Meyer TE & Tollin G (1994) A “parallel plate” electrostatic model for bimolecular rate constants applied to electron transfer proteins. *Protein Sci* **3**, 2104–2114.
- 39 Meyer TE, Zhao ZG, Cusanovich MA & Tollin G (1993) Transient kinetics of electron transfer from a variety of *c*-type cytochromes to plastocyanin. *Biochemistry* **32**, 4552–4559.
- 40 Suh JY, Tang C & Clore GM (2007) Role of electrostatic interactions in transient encounter complexes in protein-protein association investigated by paramagnetic relaxation enhancement. *J Am Chem Soc* **129**, 12954–12955.

- 41 Hazzard JT, McLendon G, Cusanovich MA & Tollin G (1988) Formation of electrostatically-stabilized complex at low ionic strength inhibits interprotein electron transfer between yeast cytochrome *c* and cytochrome *c* peroxidase. *Biochem Biophys Res Commun* **151**, 429–434.
- 42 Bernal-Bayard P, Molina-Heredia FP, Hervás M & Navarro JA (2013) Photosystem I reduction in diatoms: as complex as the green lineage systems but less efficient. *Biochemistry* **52**, 8687–8695.
- 43 Brünger AT & Karplus M (1988) Polar hydrogen positions in proteins: empirical energy placement and neutron diffraction comparison. *Proteins* **4**, 148–156.
- 44 Brooks BR, Brucoleri RE, Olafson BD, States DJ, Swaminathan S & Karplus M (1983) CHARMM: a program for macromolecular energy, minimization, and dynamics calculations. *J Comput Chem* **4**, 187–217.
- 45 MacKerell AD, Bashford D, Bellott M, Dunbrack RL, Evanseck JD, Field MJ, Fischer S, Gao J, Guo H, Ha S *et al.* (1998) All-atom empirical potential for molecular modeling and dynamics studies of proteins. *J Phys Chem B* **102**, 3586–3616.
- 46 Jurrus E, Engel D, Star K, Monson K, Brandi J, Felberg LE, Brookes DH, Wilson L, Chen J, Liles K *et al.* (2018) Improvements to the APBS biomolecular solvation software suite. *Protein Sci* **27**, 112–128.
- 47 Foerster JM, Poehner I & Ullmann GM (2018) MCMMap – a computational tool for mapping energy landscapes of transient protein-protein interactions. *ACS Omega* **3**, 6465–6475.
- 48 Metropolis N, Rosenbluth AW, Rosenbluth MN, Teller AH & Teller E (1953) Equation of state calculations by fast computing machines. *J Chem Phys* **21**, 1087–1092.
- 49 Humphrey W, Dalke A & Schulten K (1996) VMD: visual molecular dynamics. *J Mol Graph* **14**, 33–38.
- 50 Goodin DB, Davidson MG, Roe JA, Mauk AG & Smith M (1991) Amino-acid substitutions at tryptophan-51 of cytochrome *c* peroxidase – effects on coordination, species preference for cytochrome *c*, and electron-transfer. *Biochemistry* **30**, 4953–4962.
- 51 Schilder J, Lohr F, Schwalbe H & Ubbink M (2014) The cytochrome *c* peroxidase and cytochrome *c* encounter complex: the other side of the story. *FEBS Lett* **588**, 1873–1878.
- 52 Lescop E, Schanda P & Brutscher B (2007) A set of BEST triple-resonance experiments for time-optimized protein resonance assignment. *J Magn Reson* **187**, 163–169.
- 53 Battiste JL & Wagner G (2000) Utilization of site-directed spin labeling and high-resolution heteronuclear nuclear magnetic resonance for global fold determination of large proteins with limited nuclear Overhauser effect data. *Biochemistry* **39**, 5355–5365.
- 54 Gao Y, Boyd J, Williams RJP & Pielak GJ (1990) Assignment of proton resonances, identification of secondary structural elements, and analysis of backbone chemical shifts for the C102T variant of yeast iso-1-cytochrome *c* and horse cytochrome *c*. *Biochemistry* **29**, 6994–7003.
- 55 Fetrow JS & Baxter SM (1999) Assignment of ¹⁵N chemical shifts and ¹⁵N relaxation measurements for oxidized and reduced iso-1-cytochrome *c*. *Biochemistry* **38**, 4480–4492.
- 56 Volkov AN, Vanwetswinkel S, Van de Water K & van Nuland NAJ (2012) Redox-dependent conformational changes in eukaryotic cytochromes revealed by paramagnetic NMR spectroscopy. *J Biomol NMR* **52**, 245–256.
- 57 Grzesiek S, Bax A, Clore GM, Gronenborn AM, Hu JS, Kaufman J, Palmer I, Stahl SJ & Wingfield PT (1996) The solution structure of HIV-1 Nef reveals an unexpected fold and permits delineation of the binding surface for the SH3 domain of Hck tyrosine protein kinase. *Nat Struct Biol* **3**, 340–345.
- 58 Kim KL, Kang DS, Vitello LB & Erman JE (1990) Cytochrome *c* peroxidase catalyzed oxidation of ferrocyclochrome *c* by hydrogen-peroxide – ionic-strength dependence of the steady-state rate parameters. *Biochemistry* **29**, 9150–9159.
- 59 Ho PS, Hoffman BM, Solomon N, Kang CH & Margoliash E (1984) Kinetics and energetics of intramolecular electron-transfer in yeast cytochrome *c* peroxidase. *Biochemistry* **23**, 4122–4128.
- 60 Eaton JW, Bateman D, Hauberg S & Wehbring R (2020) GNU Octave Version 5.2.0 Manual: A High-Level Interactive Language for Numerical Computations. Available from: <https://www.gnu.org/software/octave/doc/v5.2.0/>
- 61 Margoliash E & Frohwirt N (1959) Spectrum of horse-heart cytochrome *c*. *Biochem J* **71**, 570–578.

Supporting information

Additional supporting information may be found online in the Supporting Information section at the end of the article.

Text S1. Simulation of the rates for the Cc:CcP_A and CcR13A:CcP_A complexes.

Fig. S1. ¹⁵N-¹H BEST-TROSY-HSQC spectra for PRE experiments.

Fig. S2. Example of chemical shift perturbation in ¹⁵N-¹H BEST-TROSY-HSQC spectra.

Fig. S3. Example of kinetics measured between CcR13A and CcP_A.

Table S1. Chemical shift perturbations (CSP) maps.

Table S2. Association rate constants (M⁻¹s⁻¹) for CcP_A and CcP_B in complex with Cc and Cc R13A.

Table S3. p-values obtained from the t-test performed by comparing the rate of association (k(II)) of the Cc:

CcP complexes at ionic strength values from 44 mM to 752 mM.

Table S4. Number of independent simulations performed to calculate the rate constants $k(\text{II})$ and used in t-test.

Table S5. Simulated rate constants for the Cc:CcP_A and CcR13A:CcP_A complexes at 122 mM ($11 \text{ mM}^{1/2}$) and 44 mM ($6.6 \text{ mM}^{1/2}$) ionic strength.